

The superconducting ‘twin’ qubit

I. V. Antonov,^{1,2} R. S. Shaikhaidarov,¹ V. N. Antonov,^{3,1,4} and O.V. Astafiev^{3,1,2}

¹Royal Holloway, University of London, Egham, TW20 0EX, UK

²National Physical Laboratory, Hampton Road Teddington, TW11 0LW, UK

³Skolkovo Institute of Science and Technology, Nobel str. 3, Moscow, 143026, Russia

⁴Moscow Institute of Physics and Technology, 29 Institutskiy per., 141700 Dolgoprudny, Moscow Region, Russia

(Dated: March 2, 2020)

In this work we study a modification of a flux qubit geometry – a combination of two loops joined by a common Josephson junction which will be called ‘twin’ qubit. At the degeneracy half-flux quantum bias in both loops, our ‘twin’ qubit has a flat energy spectrum and high anharmonicity, more than 2 GHz. This flatness makes the qubit insensitive to a global low-frequency flux noise. The qubit is capacitively coupled to a transmission line, which allows to experimentally study its spectrum. We simulate the qubit, extract its parameters with a standard quantum circuit model, compare the simulations with the experimental results.

Keywords: Flux-qubit

Superconducting qubits are among the most promising platforms for quantum computing technology. Typical qubits are on-chip aluminum structures with Josephson junctions (JJs), whose geometry can be designed to select an operating energy, state transition rates and sensitivity required in a particular environment. Over the past decade they have carried out the functionality of a transistor^{1–4}, where a control field was used to pass or block a probe field at a different frequency, multiplexer⁵, two input signals can be mixed to controllably generate a single output signal, and serial bus⁶. Superconducting qubits can be fabricated using standard nanofabrication techniques and integrated at scale into quantum circuits⁷.

One of the inherent limitations, which is encountered with superconducting qubits, is a coherence time, τ_{dec} , beyond which quantum information becomes lost. In early qubits the decoherence time was in the range of few ns. Two main sources of de-coherence are charge and flux fluctuations in vicinity of the qubit. Charge fluctuations are particular harmful for the qubits, where the charging energy, E_C , is large. In flux qubit architectures the JJ energy E_J dominates over the charging energy ($E_J/E_C \gg 1$), which lowers the device’s charge sensitivity^{8–10}. A family of flux qubit designs have led to improvement of the coherence times: shunted flux qubit¹¹, 4-JJ qubit^{12,13}.

Here we investigate experimentally a ‘twin’ qubit, consisting of two symmetrical flux qubits, linked by a common α -Josephson Junction, Fig. 1. Of particular interest to us is the weak flux dependence of the system transition energy when it is biased to the degeneracy point $\Phi_0/2$ in each loop. Compared to the original flux qubit the energy levels of the ‘twin’ qubit are very flat. A chain of 15 such qubits was recently placed into a coplanar waveguide to demonstrate flux-tunable transmission of microwaves¹⁴. In our work we isolate single ‘twin’ qubits and characterise parameters of new system in a context of application to quantum informatics. Experimental study of the transmission spectrum reveals: weak flux dependence of the transition energies close to the degeneracy point; an-

harmonicity with respect to the $|1\rangle \leftrightarrow |2\rangle$ and $|2\rangle \leftrightarrow |3\rangle$ transitions.

The sample is fabricated on an undoped silicon substrate, which is pre-patterned with 100 nm Au ground planes. We use electron beam lithography and a shadow evaporation technique to fabricate the qubit shown in Fig. 1(a). The qubit consists of five JJs integrated into two symmetrical superconducting loops. The JJs have a layered structure of Al (20 nm) - AlO_x - Al (30 nm). The energy and capacitance of the central JJ is a factor of α larger than for the outside ones, which have dimensions $400 \times 200 \text{ nm}^2$. The coplanar transmission line with impedance $Z_0 \sim 50 \Omega$ runs to the opening between the ground planes in the center of the chip. The qubits are coupled to the transmission line through T-shaped capacitors. An external magnetic field is applied to change magnetic flux bias in the identical loops.

The sample is mounted on a holder at the 13 mK stage of a dilution refrigerator. A superconducting shield is used to screen the holder from stray magnetic fields. The RF lines connected to the sample have attenuators for thermalization: -50 dBm on the 50 K stage, -30 dBm on the 4 K stage. We attach a circulator on the output line for isolation. The transmitted signal is amplified by approximately +35 dBm on the 4 K stage and by +35 dBm at room temperature. This set of attenuators and amplifiers facilitate power conversion between the laboratory equipment and the qubit. Prior to characterizing the qubit, we took the microwave transmission spectrum with the qubit detuned, and correct all measurements by subtracting background transmission profile.

Our primary goal is to study the operation of the qubit in vicinity of a double degeneracy point $\Phi_0/2$, find the intrinsic energy structure and compare with a numerical model of the system.

We study the energy spectrum of the ‘twin’ qubit by measuring transmission of coherent waves, while sweeping the biasing magnetic flux. The $|1\rangle \leftrightarrow |2\rangle$ transition, is mapped with a network analyser which measures the transmission of signal ω_{NA} through the system. Away

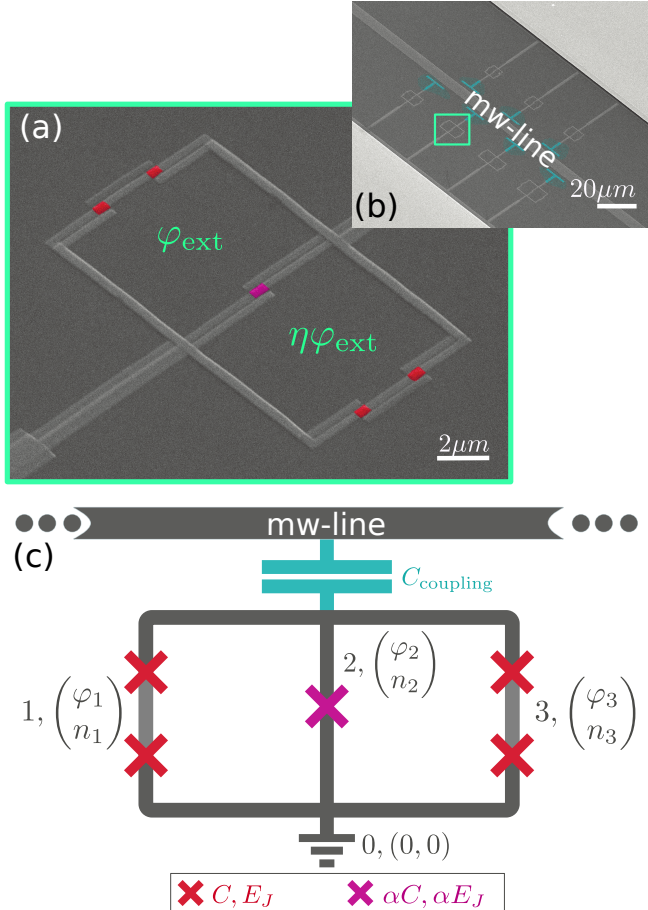


FIG. 1. Geometry of a ‘twin’ qubit: (a) Scanning electron microscope image of the ‘twin’ qubit. The Al-AlO_x-Al JJs are highlighted in red and pink; (b) Each of the qubits is coupled to the transmission line with a T-shaped capacitor; (c) The ‘twin’ qubit is a symmetrical arrangement of two individual flux qubits⁸ sharing the central JJ. Islands are labeled with a Cooper pair occupation n_i , phase φ_i , with the ground setting a reference of 0 for the variables. JJs (marked with crosses) mediate capacitive and Josephson interactions between the islands.

from resonance the signal passes through the circuit without any interaction with the qubit so that the transmission is close to 100%. Only near resonance ($\omega_{NA} = \omega_{21}$), does the qubit exchange photons with the driving field as it evolves between the ground and excited states. The qubit emits a wave that is in anti-phase with the driving field¹, so that the destructive interference in the output line results in a transmission dip, see Fig. 2(a). The plot shows power transmission $|t|^2$ obtained in a low limit drive and fitted by a Lorentzian curve with FWHM width $\Delta\omega/2\pi = 7$ MHz. This value gives us dephasing rate $\Gamma_2/2\pi \approx 3.5$ MHz.

Using the amplitude of the dip in the inset of Fig. 2(a) we can estimate coupling of our qubit to the line^{1,15}, which is characterised by the photon emission rate into the line $\Gamma_1^r = 2\Gamma_2 r_0 \approx 0.6$ MHz, where r_0 is the reflection

coefficient at the resonance.

The transmission minimum at different magnetic fields maps out the qubit’s ω_{21} transition spectrum, Fig. 2(a). Such a spectrum is observed in vicinity of external flux bias $\Phi \approx \Phi_0/2$ for all samples. Because of a small asymmetry, $\eta \approx 1$, the fluxes linked through the left and right loops can be slightly different: Φ and $\eta\Phi$, correspondingly. This results in gradual change of transmission frequency at large magnetic field, Fig 2(b).

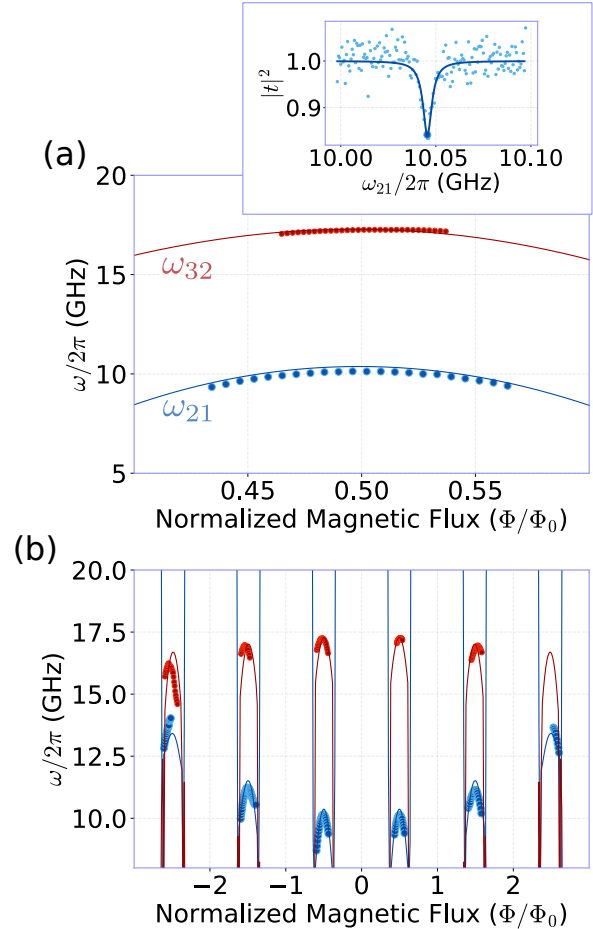


FIG. 2. Spectrum of the quantum system. (a) The resonance frequencies, ω_{21} , in the vicinity of $\Phi_0/2$ (blue points). An inset exemplifies the power transmission coefficient $|t|^2$ for the $|1\rangle \leftrightarrow |2\rangle$ transition. The transition frequencies ω_{32} (red) are obtained in a two-tone measurement. (b) The spectrum measured in a wide flux bias range. Experimental data (circles) are compared with simulations (solid lines) for ω_{21} (blue) and ω_{32} (red). Asymmetry in the flux penetrating the left and right loops results in the gradual change of transition frequencies with every Φ_0 period: ω_{21} creeps up, while ω_{32} creeps down, breaking the usual periodicity of flux qubits.

The $|2\rangle \leftrightarrow |3\rangle$ transition, ω_{32} , is mapped using spectroscopy with two tones. The network analyzer probes signals at ω_{21} , while an additional generator sweeps a second frequency, ω_{GEN} . Whenever the second tone from the generator hits the $|2\rangle \rightarrow |3\rangle$ transition ($\omega_{GEN} = \omega_{32}$), the qubit undergoes a ladder of excitations, $|1\rangle \xrightarrow{\omega_{21}} |2\rangle$

$\xrightarrow{\omega_{32}}$ |3⟩, depopulating states |1⟩ and |2⟩. Because of this depopulation, the probe signal at ω_{21} is modified. This identifies ω_{32} , which is mapped with red circles, see Fig 2(b). One can note that the qubit has a large anharmonicity in the two lowest transitions of more than 7.5 GHz.

We match the experimental data to the theoretical model: Islands, isolated by the JJ in Fig. 1, are labeled with Cooper pair (CP) occupation $\vec{n} = |n_1, n_2, n_3\rangle$, and phase $\vec{\varphi} = |\varphi_1, \varphi_2, \varphi_3\rangle$. The charges and potentials on the islands are linked by the capacitance matrix:

$$2e\vec{n} = \mathbf{C}\vec{V}. \quad (1)$$

The capacitance matrix in the ‘twin’ qubit topology is (see Supplementary Note I):

$$\mathbf{C} = C \begin{pmatrix} 2 & -1 & 0 \\ -1 & 2 + \alpha & -1 \\ 0 & -1 & 2 \end{pmatrix}, \quad (2)$$

where C is the capacitance of the outer JJs. The interaction of the CPs, carrying a charge $\vec{Q} = 2e\vec{n}$, and potentials on their respective islands gives rise to the kinetic energy term (considering vortex motion) of the Hamiltonian:

$$T = E_C C \vec{n}^T \mathbf{C}^{-1} \vec{n}, \quad (3)$$

where charging energy is $E_C = (2e)^2/2C$.

Each JJ with a phase difference of $\Delta\varphi_i$, contributes $E_{Ji}[1 - \cos(\Delta\varphi_i)]$ to a Josephson potential. Additional phase due to external magnetic flux is accounted as an additional phase in left and right loops φ_{ext} and $\eta\varphi_{\text{ext}}$:

$$U = E_J [4 + \alpha - \alpha \cos(\varphi_2) - \cos(\varphi_1) - \cos(\varphi_3) - \cos(\varphi_2 - \varphi_1 - \varphi_{\text{ext}}) - \cos(\varphi_2 - \varphi_3 + \eta\varphi_{\text{ext}})]. \quad (4)$$

Here η is a factor close but slightly different from one due to small asymmetry in the loop geometries.

The Hamiltonian, $\mathcal{H} = T + U$, is written in the charge basis (see Supplementary Note II) with $E_J/h = 91.0 \text{ GHz}$, $E_C/h = 13.5 \text{ GHz}$, $\alpha = 1.023$, $\eta = 1.011$. The resulting eigenenergies are compared with the experimental data in Fig. 2(b). Data for ω_{32} is taken in a limited flux range, $0.4\Phi_0$ and above $0.6\Phi_0$, because away from $\Phi = (n + \frac{1}{2})\Phi_0$, $n \in \mathbb{Z}$, the energy of $|1\rangle \leftrightarrow |2\rangle$ diverges. The asymmetry value, η , is close to the 3% seen from the SEM image in Fig. 1. The resonance is periodic in flux, with a tendency of higher ω_{21} at higher magnetic flux numbers, because of the loop asymmetry.

An important parameter of the ‘twin’ qubit is the curvature at the operation point of the qubit, $\Phi_0/2$. A low curvature is desirable, because it makes the qubit less sensitive to external flux changes and improves decoherence time. At the ‘twin’ qubits’ degeneracy points $\Phi = (n + \frac{1}{2})\Phi_0$, $n \in \mathbb{Z}$, the curvature is $(-550 \pm 10) \text{ GHz}/\Phi_0^2$. It is substantially smaller than for 3-JJ and 4-JJ flux qubits with similar JJ parameters^{1,16,17}, where the curvature is of the order of $10^5 \text{ GHz}/\Phi_0^2$.

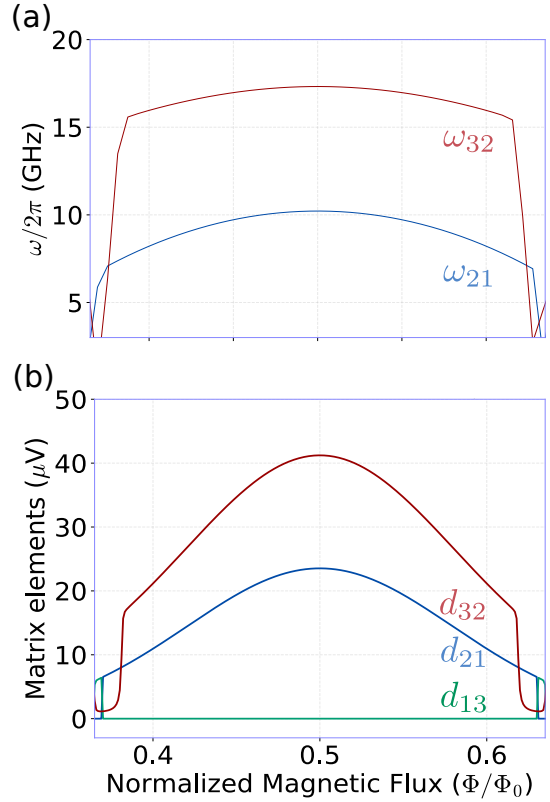


FIG. 3. **Modelling the qubit.** (a) Calculations of transmission frequencies for the symmetric qubit, $\eta = 1$. (b) Transition matrix elements $|d_{12}|$, $|d_{13}|$ and $|d_{21}|$ for the central island (Fig 1).

Figure 3 shows simulation results for an ideal case of fully symmetric system ($\eta = 1$). The curves are exactly periodic in magnetic field with period of Φ_0 , therefore only one period is shown. The operational range of the qubit lies approximately from 0.43 to 0.57 of Φ_0 , where α -junction is in the superposed 0- π state¹⁴. Away from that range the transition frequency ω_{21} diverges.

In addition, we analyse ‘optical’ properties of our qubit. Particularly, matrix elements $d_{12} = \langle 1 | \hat{V}_2 | 2 \rangle$, $d_{13} = \langle 1 | \hat{V}_2 | 3 \rangle$ and $d_{21} = \langle 2 | \hat{V}_2 | 3 \rangle$ with physical meaning of induced potential on the island 2 due to atomic transitions between levels 1-2, 1-3 and 2-3 are calculated and plotted in Fig. 3(b). Here $\hat{V}_2 = (2e)^{-1} \partial H / \partial n_2$ is the potential operator for the island 2. It characterises coupling of the qubit to the field of propagating waves in the line, as well as its quantum fluctuations, responsible for photon emission. The calculation of the operator is given in Supplementary Note III. It is interesting that $d_{13} = 0$ for a wide magnetic flux interval, oppositely to a flux qubit where it happens strictly at the degeneracy point $\Phi_0/2$ only. This is due to symmetry of the system (two loops) to the external flux.

We estimate the photon emission rate using relationship^{1,15} $\Gamma_1^r = (d_{12} C_k)^2 \omega Z_0 / \hbar$ and found that the previously estimated value ($\Gamma_1^r / 2\pi = 0.6 \text{ MHz}$)

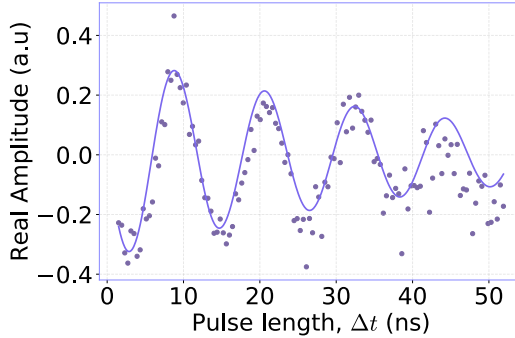


FIG. 4. Rabi oscillations: taken at the degeneracy point by driving the qubit with resonant microwaves pulses for fixed time periods, Δt . The decoherence time of $\tau_{\text{dec}} = 42$ ns is extracted from the decay envelope, $e^{-\Delta t/\tau_{\text{dec}}}$, of the the oscillations.

can be obtained if we substitute coupling capacitance $C_c = 6$ fF, which is very reasonable value for our geometry.

Finally, we measure Rabi oscillations, see Fig. 4 by ap-

plying short microwave pulses with varied length. The oscillations decay with characteristic time $\tau_{\text{dec}} = 42$ ns (Fig. 4), It is consistent with the decoherence time taken from the spectroscopy measurements $\Gamma_2 \approx 1/\tau_{\text{dec}} \approx 2\pi \times 3.8$ MHz. A relatively short decoherence time in our experiment is not surprising and can be a result of poisoning of the sample with the infrared radiation, and the coupling of the qubit to the two-level oscillators in the substrate, owing to the simplified technology used in the qubit's fabrication. Note also that coherent operation is additionally limited due to strong coupling to the open line.

In conclusion, we have fabricated and characterised an isolated ‘twin’ qubit. With this geometry the qubit has weak flux sensitivity at the degeneracy point and strong anharmonicity. The measured energy level structure is well reproduced by the numerical model.

ACKNOWLEDGEMENT

The work was supported by the grants EP-SRC EP/T004088/1, H2020-FETOPEN-2018 QUANTUM E-LEAPS and RSF No. 16-12-00070.

-
- ¹ O. Astafiev, A. M. Zagoskin, A. A. Abdumalikov, Y. A. Pashkin, T. Yamamoto, K. Inomata, Y. Nakamura, and J. S. Tsai, *Science* **327**, 840 (2010).
 - ² I.-C. Hoi, C. M. Wilson, G. Johansson, T. Palomaki, B. Peropadre, and P. Delsing, *Physical Review Letters* **107** (2011), 10.1103/physrevlett.107.073601.
 - ³ A. A. Abdumalikov, O. Astafiev, A. M. Zagoskin, Y. A. Pashkin, Y. Nakamura, and J. S. Tsai, *Physical Review Letters* **104** (2010), 10.1103/physrevlett.104.193601.
 - ⁴ O. V. Astafiev, A. A. Abdumalikov, A. M. Zagoskin, Y. A. Pashkin, Y. Nakamura, and J. S. Tsai, *Physical Review Letters* **104** (2010), 10.1103/physrevlett.104.183603.
 - ⁵ T. Höngl-Decrinis, I. V. Antonov, R. Shaikhaidarov, V. N. Antonov, A. Y. Dmitriev, and O. V. Astafiev, *Physical Review A* **98** (2018), 10.1103/physreva.98.041801.
 - ⁶ J.-T. Shen and S. Fan, *Physical Review Letters* **95** (2005), 10.1103/physrevlett.95.213001.
 - ⁷ M. W. Johnson, P. Bunyk, F. Maibaum, E. Tolkacheva, A. J. Berkley, E. M. Chapple, R. Harris, J. Johansson, T. Lanting, I. Perminov, E. Ladizinsky, T. Oh, and G. Rose, *Superconductor Science and Technology* **23**, 065004 (2010).
 - ⁸ T. P. Orlando, J. E. Mooij, L. Tian, C. H. van der Wal, L. S. Levitov, S. Lloyd, and J. J. Mazo, *Physical Review Letters* **109** (2012), 10.1103/physrevlett.109.010502.
 - ⁹ I. Chiorescu, *Science* **299**, 1869 (2003).
 - ¹⁰ J. E. Mooij, *Science* **285**, 1036 (1999).
 - ¹¹ F. Yan, S. Gustavsson, A. Kamal, J. Birenbaum, A. P. Sears, D. Hover, T. J. Gudmundsen, D. Rosenberg, G. Samach, S. Weber, J. L. Yoder, T. P. Orlando, J. Clarke, A. J. Kerman, and W. D. Oliver, *Nature Communications* **7** (2016), 10.1038/ncomms12964.
 - ¹² Y. Qiu, W. Xiong, X.-L. He, T.-F. Li, and J. Q. You, *Scientific Reports* **6** (2016), 10.1038/srep28622.
 - ¹³ I. M. Pop, K. Geerlings, G. Catelani, R. J. Schoelkopf, L. I. Glazman, and M. H. Devoret, *Nature* **508**, 369 (2014).
 - ¹⁴ K. V. Shulga, E. Il'ichev, M. V. Fistul, I. S. Besedin, S. Butz, O. V. Astafiev, U. Hübner, and A. V. Ustinov, *Nature Communications* **9** (2018), 10.1038/s41467-017-02608-8.
 - ¹⁵ Z. H. Peng, S. E. de Graaf, J. S. Tsai, and O. V. Astafiev, *Nature Communications* **7** (2016), 10.1038/ncomms12588.
 - ¹⁶ M. Stern, G. Catelani, Y. Kubo, C. Grezes, A. Bienfait, D. Vion, D. Esteve, and P. Bertet, *Physical Review Letters* **113** (2014), 10.1103/physrevlett.113.123601.
 - ¹⁷ S. Gustavsson, F. Yan, J. Bylander, F. Yoshihara, Y. Nakamura, T. P. Orlando, and W. D. Oliver, *Physical Review Letters* **109** (2012), 10.1103/physrevlett.109.010502.